Recoil-corrected continuum shell model calculations for ^{11}B(p,n)^{11}C, ^{11}B(p,p')^{11}B*, ^{12}C(e,$e'x$)

Dean Halderson
Department of Physics, Western Michigan University, Kalamazoo, Michigan 49008, USA
(Received 15 November 2012; revised manuscript received 17 May 2013; published 19 July 2013)

Background: The recoil-corrected continuum shell model provides coupled-channels solutions for bound and unbound wave functions from realistic effective interactions. The wave functions are antisymmetric and contain no spurious components because the calculations are performed in the center-of-mass system.
Purpose: This model has now been extended to include $1\hbar\omega$ excitations in the structure of p-shell target (residual) nuclei, hence allowing $0s$-shell knockout processes. Several reactions involving the ^{12}C compound system are investigated to demonstrate the utility of the model.
Methods: The states of ^{11}B and ^{11}C are constructed in the nonspurious $0\hbar\omega$ plus $1\hbar\omega$ model space. An interaction, fitted to Cohen and Kurath (8-16) plus Reid soft core g-matrix elements, is employed. One nucleon is coupled to these states to create a basis for the bound and scattering states for ^{12}C.
Results: Calculated elastic and inelastic cross sections agree well with available data. The calculated transverse response at high momentum transfer is lower than that extracted from data. Although significant, meson exchange currents are not sufficient to give agreement with data. Likewise inclusion of $0s$-shell knockout is not sufficient to provide agreement. The high-energy octupole resonance appears at low momentum transfer and an energy of $106/A^{1/3}$.
Conclusions: The model should provide meaningful predictions for states near the proton drip line via the (p,n) reaction. Coupled-channels solutions are necessary for describing ^{12}C(e,$e'x$) at low momentum transfer. Lack of strength at low energy and momentum transfer in optical model calculations of ^{12}C(e,$e'x$) is at least partly attributable to the omission of giant resonances. Data for $(\pi^+,\pi^{+\prime}p)/(\pi^-,\pi^{-\prime}p)$ could verify this conclusion. Lack of strength in the transverse response may be attributable to recoil terms which are omitted in most calculations.

DOI: 10.1103/PhysRevC.88.014610 PACS number(s): 25.30.Fj, 25.40.Cm, 25.40.Ep, 25.40.Kv

I. INTRODUCTION

Reactions involving one nucleon in the continuum, such as elastic and inelastic nucleon-scattering, charge-exchange, and knockout reactions, are conveniently investigated in continuum shell-model calculations. The processes can be analyzed and described in conventional shell-model terms. The recoil-corrected continuum shell model (RCCSM) [1,2] has the advantage of producing wave functions that are antisymmetric and contain no spurious components because the calculations are performed in the center-of-mass system. Any realistic effective interaction may be employed as long as it is translationally invariant. Solutions are obtained by the **R** matrix method [3], which has proven to be the most physical and convenient reaction theory for solving many-coupled channel systems in light- and medium-mass nuclei. It is not uncommon to couple 30 or more residual states of the target. In addition to providing scattering states, the formalism yields bound states and resonances. Coupled-channels techniques which involve integrating coupled differential equations can become unstable for large numbers of channels, and they can miss narrow resonances because the equations must be solved for each energy over the resonance. Additional advantages of the **R** matrix procedure may be found in a review article by Descouvemont [4].

The RCCSM has been applied to several nuclei with the core (target or residual) states restricted to the p shell [5,6]. The structure of the core states has now been extended to include the p-shell plus one-particle excitations from the $0s$ to $0p$ shell and one-particle excitations from the $0p$ to the sd shell.

The purpose of this article is to pick a system near the middle of the p shell for which numerous data exist and to see how the model results compare to these data. Certainly no nucleus has been investigated more than ^{12}C. Success in describing reactions for this compound system will be a test of the model's ability to predict other reactions in other systems. The model does very well for elastic and inelastic proton scattering and (p,n) reactions. It should, therefore, make reasonable predictions for systems near the proton drip line. The (e,$e'p$) and (e,$e'x$) results give reasonable agreement at low momentum transfer. It is shown that, in this momentum transfer region, coupled-channels solutions are required for agreement with data and that a true structure model that produces resonances is required. Appearing at an energy of $106/A^{1/3}$ MeV is the high-energy octupole resonance. The inclusion of the $0s$ shell knockout is less significant, but appreciable throughout the 300–500 MeV/c range of momentum transfer. At high momentum transfer the effect of coupled channels and structure become less important. However, meson exchange currents (MECs) persist at higher momentum and energy transfer, but their inclusion is not sufficient to provide agreement with the extracted transverse response function. This is in contrast to ^{4}He(e,$e'x$), where inclusion of the MEC contribution provided agreement with data. A possible explanation for the deficit in the transverse response is the omission of recoil terms.

II. THE MODEL

The input to the RCCSM is an oscillator size parameter, $\upsilon_0 = m\omega/\hbar$ (0.32 fm^{-2} in this work), the desired states of the $A-1$ core nuclei, and a realistic, translationally invariant interaction. Wave functions and scattering observables are calculated with **R** matrix techniques. For p-shell nuclei [7] the channel wave functions within the channel radius, a_c, may be written as an expansion in a harmonic oscillator basis,

$$\Psi_{J_B} = \sum_{J_A\alpha\bar{l}\bar{j}\bar{n}} f_{\bar{n}\bar{l}\bar{j}J_A\alpha J_B}\left[a^+_{\bar{n}\bar{l}\bar{j}} \otimes |\alpha J_A\rangle\right]^{J_B} + \sum_\beta d_\beta\,|\beta J_B\rangle\,, \tag{1}$$

where β runs over all $0\hbar\omega$, p-shell states with spin J_B and $a^+_{\bar{n}\bar{l}\bar{j}}$ creates a particle in the core-nucleon, center-of-mass coordinate. The sum over $\bar{n}$ and $\bar{l}$ goes to $\bar{n}+\bar{l}=22$ in this calculation, where $\bar{n}$ starts at zero. The created particles are coupled to chosen nonspurious $0\hbar\omega$ plus $1\hbar\omega$ states of the $A-1$ core. These states are labeled by $|\alpha J_A\rangle$ and designate the channels to be coupled.

The wave function with outgoing flux v_i with initial conditions $i=\{\alpha J_A M_A m_s\}$ takes the form [8]

$$\psi^{(-)}_i = (4\pi/p_i)\sum i^\ell Y^*_{\ell m_\ell}(\hat{p})e^{-i\sigma_\ell}(-i/2) \times C^{\ell 1/2 j}_{m_\ell m_s m} C^{J_A j J_B}_{M_A m M_B}\Psi^{J_B M_B(-)}_c, \tag{2}$$

where the sum is over $\ell m_\ell j m J_B M_B$ and

$$\Psi^{J_B M_B(-)}_c = \sum_{c'} r^{-1} u^{J_B(-)}_{c'}(r)|\alpha' J'_A \ell' j' J_B M_B\rangle. \tag{3}$$

The radial function $u^{J_B(-)}_{c'}$ has the asymptotic form

$$u^{J_B(-)}_{c'} = u^{J_B(+)*}_{c'} \to (v_c/v_{c'})^{1/2}(O_{c'}\delta_{cc'} - I_{c'}S_{cc'}). \tag{4}$$

The index c stands for $\alpha J_A \ell j$ with J_A and j coupled to J_B, and p_i is the nucleon momentum in the nucleon-nucleus center-of-mass frame.

The required energies, overlaps, and one-body densities of the p-shell states were calculated with the code NUSHELL [9]. The interaction was derived from a fit to Cohen and Kurath (8-16) [10] (CK) and the Reid soft-core [11] g-matrix elements for ^{16}O. The matrix elements are fit to a sum of Yukawas. The interaction is shown in the Appendix. It contains central, spin-orbit, and tensor components, but no antisymmetric spin-orbit. A comparison with the CK matrix elements is shown in Table I. The matrix elements show a similar trend, but the form of the parameterization, the requirement that the high $\hbar\omega$ Reid matrix elements be fit, plus the lack of an antisymmetric spin-orbit component means the fit cannot account for the more extreme values of the CK matrix elements.

Hence, the calculated low-lying spectrum for ^{11}B, shown in Fig. 1, has the $7/2^-$ state out of order. In addition, the $1/2^+$ state comes too high. In a conventional bound-state shell model, this would be corrected by changing the sd single-particle energies. However, in the RCCSM the single-particle energies are calculated from the interaction. Therefore, the threshold for $0s$ shell knockout will be about 3 MeV too high.

TABLE I. Comparison of the CK(8-16) matrix elements with those obtained from the interaction in this work. The i, j, m, and n orbits may be $1=p_{1/2}(p)$, $2=p_{3/2}(p)$, $3=p_{1/2}(n)$, or $4=p_{3/2}(n)$. The matrix elements are in MeV.

i	j	m	n	J	CK	Present
1	1	1	1	0	0.24	0.92
2	1	2	1	1	0.73	0.59
2	1	2	1	2	−1.14	−1.5
2	2	1	1	0	−5.05	−4.4
2	2	2	1	2	−1.74	−1.6
2	2	2	2	0	−3.33	−2.19
2	2	2	2	2	0.09	−0.37
3	3	3	3	0	0.24	0.43
4	3	4	3	1	0.73	0.16
4	3	4	3	2	−1.14	−1.97
4	4	3	3	0	−5.05	−4.48
4	4	4	3	2	−1.74	−1.63
4	4	4	4	0	−3.33	−2.73
4	4	4	4	2	0.09	−0.82
1	3	1	3	0	0.24	0.43
1	3	1	3	1	−4.29	−1.99
2	3	1	3	1	1.2	1.39
1	4	1	3	1	−1.2	−1.39
2	3	2	3	1	−6.56	−4.44
2	3	2	3	1	0.73	0.16
2	3	2	3	2	−4.06	−3.42
2	3	2	3	2	−1.14	−1.97
2	4	1	3	0	−5.05	−4.48
2	4	1	3	1	1.77	0.6
2	4	2	3	1	3.21	2.15
2	4	1	4	1	−3.21	−2.15
2	4	2	3	2	−1.74	−1.63
2	4	1	4	2	1.74	1.63
2	4	2	4	0	−3.33	−2.73
2	4	2	4	1	−3.44	−1.39
2	4	2	4	2	0.09	−0.82
2	4	2	4	3	−7.27	−3.93

In Eq. (1) the only positive-parity $A=11$ states that are included are the $1/2^+$ states because this work is mainly interested in the contribution of the $0s$ shell knockout. The nonspurious $1/2^+$ states contain 9/11 of the $0s$ hole state and this $0s$ hole state strength is distributed as in Fig. 2 in ^{11}B. We take the first four states of ^{11}B and ^{11}C, and hence 90% of the available $0s$ hole strength. This violates the empirical RCCSM rule that one should choose only core states that correspond to states that are experimentally nucleon bound or nearly bound. Following this rule, one should take only two of each. However, the inclusion of four each would represent the maximum contribution of the $0s$ hole states in the energy region of interest. Inclusion of four instead of two produces some unphysical resonances at high excitation energy, as seen in the following section. In addition to the four $1/2^+$ states, the negative-parity states, $1/2^-_1$, $1/2^-_2$, $1/2^-_3$, $3/2^-_1$, $3/2^-_2$, $3/2^-_3$, $5/2^-_1$, $5/2^-_2$, $5/2^-_3$, $7/2^-_1$, and $7/2^-_2$, of ^{11}B and ^{11}C were included as $|\alpha J_A\rangle$ states.

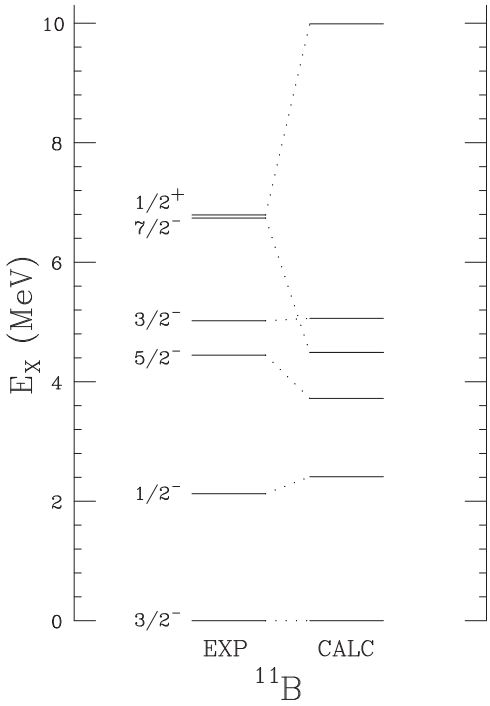

FIG. 1. The low-lying states of ^{11}B.

III. INELASTIC SCATTERING

Data are available for the ^{11}B$(p,n)^{11}$C and ^{11}B$(p,p')^{11}$B in a proton energy region suitable for investigating rare isotopes by inverse kinematics. The ^{11}B$(p,n)^{11}$C cross sections to the ground state and first $1/2^-$ state for 30- and 50-MeV proton energies are shown in Fig. 3 with the data of Ref. [12] The agreement with the data is good, demonstrating that the structure of these states and the interaction are modeling the process well.

In Fig. 4 are shown the ^{11}B$(p,p')^{11}$B cross sections to the first $1/2^-$, $5/2^-$, and $7/2^-$ states and the second $3/2^-$ state

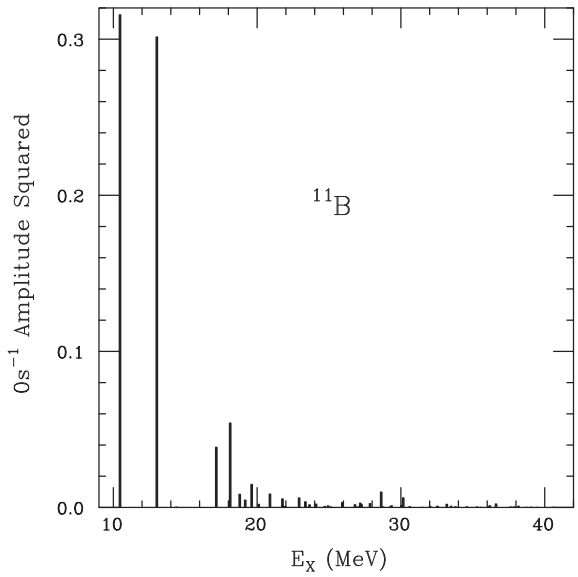

FIG. 2. Distribution of 0s hole strength in ^{11}B.

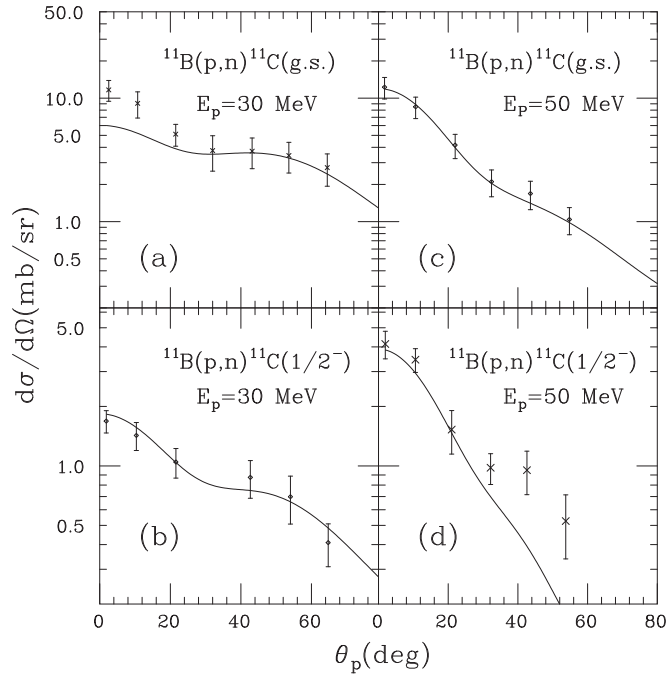

FIG. 3. Charge-exchange cross sections for ^{11}B to the ground state and first excited state of ^{11}C. The solid lines are from calculations. The data are from Ref. [12].

along with the data of Ref. [13]. Again the agreement with data is good for the $1/2^-$, $5/2^-$, and $7/2^-$ states, showing that the structure of these states is well modeled and that the contributing components of the interaction are appropriate. The agreement for the second $3/2^-$ state is less satisfactory, indicating that the state may have higher order structure

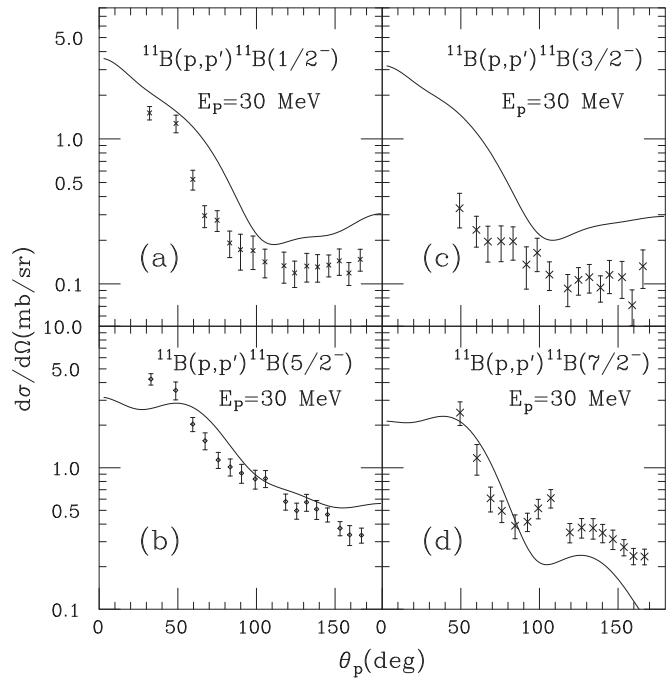

FIG. 4. Inelastic scattering of protons from ^{11}B. Solid curves are from RCCSM calculations. Data are from Ref. [13].

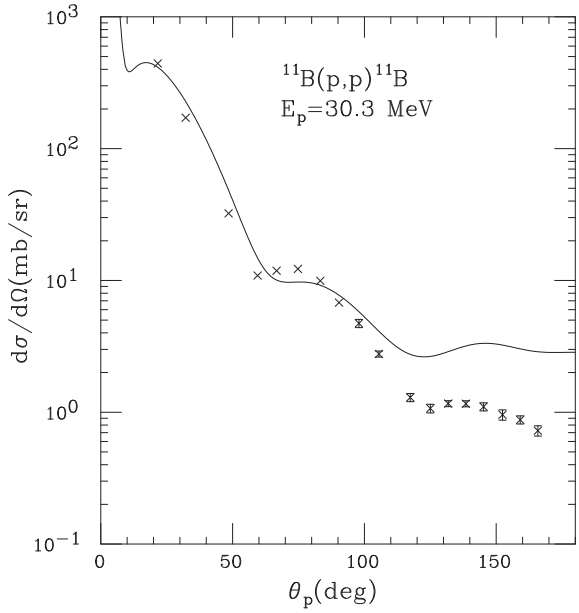

FIG. 5. Elastic proton scattering from ^{11}B at 30.3 MeV. The solid line is the RCCSM calculation. Data are from Ref. [14].

components. The four calculated curves agree as well or better with the data than those of the intermediate coupling model in Ref. [13].

IV. ELASTIC SCATTERING

Elastic proton scattering data are available at 30.3 and 155 MeV. These results are shown in Figs. 5 and 6 with the data of Refs. [14] and [15], respectively. The agreement with the 30.3-MeV data is good; in fact, the quality of the agreement is similar to the optical model fits in Ref. [14]. The

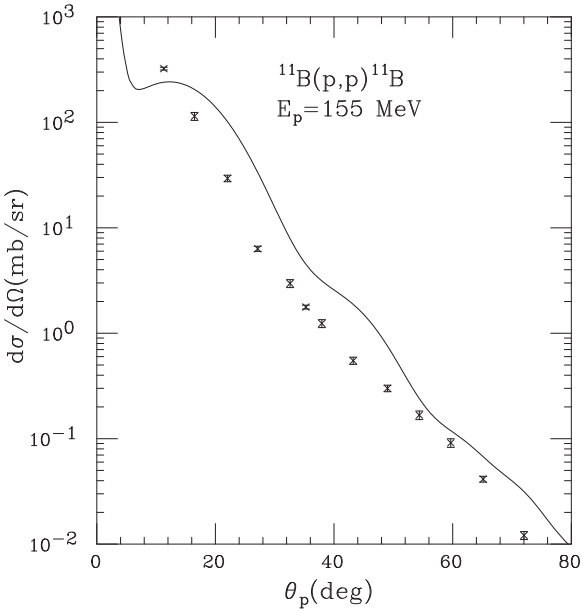

FIG. 6. Elastic proton scattering from ^{11}B at 155 MeV. The solid line is the RCCSM calculation. Data are from Ref. [15].

155-MeV calculation show less agreement with the data. This calculated cross section is surprisingly insensitive to changes in the interaction and the allowed ^{11}B configurations as long as the long-range component of the effective interaction is fixed at the one-pion exchange. This means a mechanism must be missing from the model, and that mechanism is the two-nucleon knockout. Therefore, without adding absorption into the two-body interaction, one expects the elastic cross section to be overpredicted for energies above 100 MeV. However, the qualitative agreement at 155 MeV is not of concern because knockout reactions show less sensitivity to the interaction at high-energy transfer. Therefore, the RCCSM is one model that will provide satisfactory agreement with many nucleon-induced reactions at moderate energies and sufficient agreement for intermediate-energy reactions.

V. THE ^{12}C(e,$e'x$) REACTION

Many experiments and numerous calculations have been performed for this reaction [16]. Fermi-gas calculations were among the first [17]. These calculations could provide reasonable agreement with extracted longitudinal responses at moderate momentum transfer, but at the expense of overpredicting the longitudinal response at low-momentum transfer. In an attempt to explain the overestimate of the longitudinal response in these Fermi-gas calculations, a number of continuum random phase approximation (RPA) calculations followed [18–20]. The calculation of Ref. [18] improved the longitudinal responses, but they were still overestimated, while the transverse responses were too low. A number of relativistic calculations followed [21,22], some of which included vacuum polarization. An improvement in the longitudinal response was obtained, but calculations were limited to the higher momentum transfers.

The difficulty with the RPA calculations is that they tend to be sensitive to the interaction, and without proton scattering calculations, it is difficult to judge the appropriateness of each interaction. The calculation in Ref. [23] took a step toward addressing this problem by coupling shell-model states to optical model solutions for outgoing protons and neutrons. Calculations were performed with and without distortion. Those with distortion provided reasonable longitudinal responses, but underpredicted the transverse responses. A recent ^{4}He(e,$e'x$) self-consistent continuum RPA calculation also found that the transverse responses were too low [24]. Therefore, a general trend is that calculations that reproduce the longitudinal response in the quasielastic region, underpredict the transverse response at high-momentum transfer.

It will be helpful to have calculations from a coupled-channels model that is successful in describing nucleon induced reactions. We follow Ref. [25], where $\hbar = c = 1$. The incident and exit electron momenta are $k_\mu = (k_0, \mathbf{k})$ and $k'_\mu = (k'_0, \mathbf{k}')$; the final, free nucleon momentum is $p_\mu = (p_0, \mathbf{p})$; the final core momentum is $p_{A\mu} = (E_A, \mathbf{p}_A)$; and the momentum transferred to the nucleus is $q_\mu = (q_0, \mathbf{q}) = k'_\mu - k_\mu$. For inclusive scattering one sums over all possible outgoing channels. This allows one to write the cross section

as [8]

$$\frac{d^2\sigma}{d\Omega d\omega} = \frac{1}{2\pi}\sum_{c,J_B}(\mu_c/p_c)\frac{d\sigma_{cJ_B}}{d\Omega}, \tag{5}$$

where $d\sigma_{cJ_B}/d\Omega$ is a fictitious cross section calculated with the wave functions in Eq. (2) with outgoing flux v_c in open channel c. The equation for $d\sigma_{cJ_B}/d\Omega$ in the laboratory frame can be taken as Eq. (3.46) in Ref. [26]. For exclusive scattering to a definite residual nuclear state, the cross section is given by

$$\frac{d^5\sigma}{d\Omega d\Omega_p d\omega} = \frac{\alpha^2}{q_\mu^4}\left(\frac{2k_0' p_0 p}{k_0 R}\right)\left(k_\mu k_\nu' + k_\mu' k_\nu + q_\mu^2 g_{\mu\nu}/2\right)J^\mu J^{\nu *}, \tag{6}$$

where α is the fine structure constant and $R = (1 - p_0\mathbf{p}\cdot\mathbf{p}_A/p^2E_A)$.

Because all nucleon and nucleus angular momentum projections will be summed over and the initial nuclear state has spin zero ($J_B = 0$), the spherical components of the nuclear currents for all final projections, M_B', may be written as

$$J_\lambda = -(2\pi)^{1/2}(-i)^J\langle J_B'\| - T_j^{\rm el} + \lambda T_J^{\rm mag}\| J_B = 0\rangle\delta_{JJ_B'} \tag{7}$$

for $\lambda = \pm 1$,

$$J_{\lambda=0} = J_z = -(4\pi)^{1/2}(-i)^J\langle J_B'\| L_J\| J_B = 0\rangle\delta_{JJ_B'}, \tag{8}$$

$$J_0 = -(4\pi)^{1/2}(-i)^J\langle J_B'\| M_J^{\rm Coul}\| J_B = 0\rangle\delta_{JJ_B'}. \tag{9}$$

The continuity equation, $q_\mu J^\mu = 0$, is employed to eliminate J_z in favor of $(q_0/q)\rho$. In a nonrelativistic reduction of the current operators we keep only terms of order $1/M_N$, yielding

$$M_{JM}^{\rm Coul} = \sum_i j_J(qr_i)Y_{JM}(\hat{r}_i)F_1^i(q_\mu^2), \tag{10}$$

$$T_{JM}^{\rm el} = \sum_c\left(F_1^i(q_\mu^2)/M_N\right)\left\{-\left(\frac{J}{2J+1}\right)^{1/2} j_{J+1}(qr_i)[Y_{J+1}(\hat{r}_i)\otimes\vec{\nabla}_i]_{JM} + \left(\frac{J+1}{2J+1}\right)^{1/2} j_{J-1}(qr_i)[Y_{J-1}(\hat{r}_i)\otimes\vec{\nabla}_i]_{JM}\right\}$$
$$+\left[F_1^i(q_\mu^2) + \kappa_i F_2^i(q_\mu^2)\right][q/(2M_N)]j_J(qr_i)[Y_J(\hat{r}_i)\otimes\sigma_i]_{JM}, \tag{11}$$

$$T_{JM}^{\rm mag} = \sum_c (iq)\left\{-\left(\frac{J}{2J+1}\right)^{1/2} j_{J+1}(qr_i)[Y_{J+1}(\hat{r}_i)\otimes\sigma_i]_{JM} + \left(\frac{J+1}{2J+1}\right)^{1/2} j_{J-1}(qr_i)[Y_{J-1}(\hat{r}_i)\otimes\sigma_i]_{JM}\right\}$$
$$\times\left[F_1^i(q_\mu^2) + \kappa_i F_2^i(q_\mu^2)\right]/(2M_N) - \left[iF_1^i(q_\mu^2)/M_N\right]j_J(qr_i)[Y_J(\hat{r}_i)\otimes\vec{\nabla}_i]_{JM}. \tag{12}$$

Transverse and longitudinal responses for a spin zero initial state are given by

$$R_T = \sum_{J=1}(|\langle J_B'\|T_j^{\rm el}\|J_B = 0\rangle|^2 + \langle J_B'\|T_J^{\rm mag}\|J_B = 0\rangle|^2), \tag{13}$$

$$R_L = \sum_{J=0}|\langle J_B'\|T_j^{\rm Coul}\|J_B = 0\rangle|^2. \tag{14}$$

The nucleon form factors are taken from the three-pole approximation of Ref. [27].

The MECs of Ref. [28] are also calculated, but in the approximation that no $0s^40p^8$ components appear in the scattering states wave functions. This should be a very good approximation for the energy range considered.

In Fig. 7 are shown the inclusive data of Ref. [29] at $E_e =$ 1500 MeV and $\theta = 11.95^\circ$ and in Fig. 8 of Ref. [30] at $E_e =$ 480 MeV and $\theta = 36^\circ$ compared to the calculated results for neutron plus proton knockout, both with (dashed line) and without MEC (solid line). Both of these data sets correspond to an average momentum transfer of $\sim$300 MeV/c. Owing to the large bin size, the data will not show the low-lying resonances.

The spike at $\omega = 100$ MeV and apparent weak resonances at higher energy appearing in the calculation are attributable to collective spin excitations built on the four nonphysical $1/2^+$ core states, as mentioned above. Eliminating them from the basis removes the effect. However, the resonance at $\omega =$ 47 MeV is real and remains even when all eight $1/2^+$ core

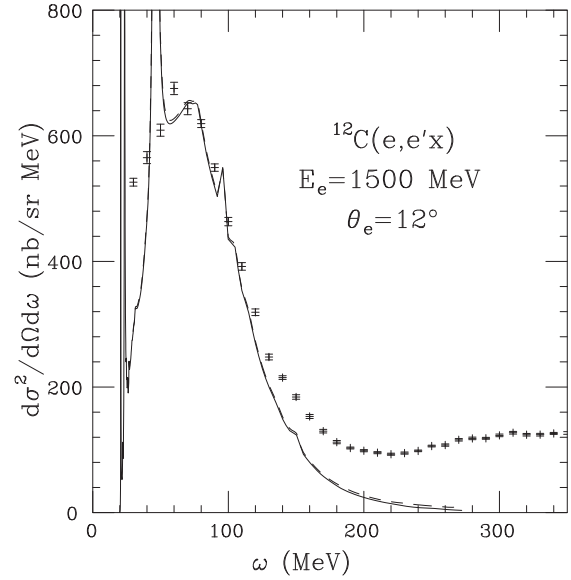

FIG. 7. Cross section for ^{12}C(e,$e'x$). The solid curve is from calculation with single-particle operators [Eqs. (10)–(12)]. The dashed curve includes meson exchange contribution. Data are from Ref. [29].

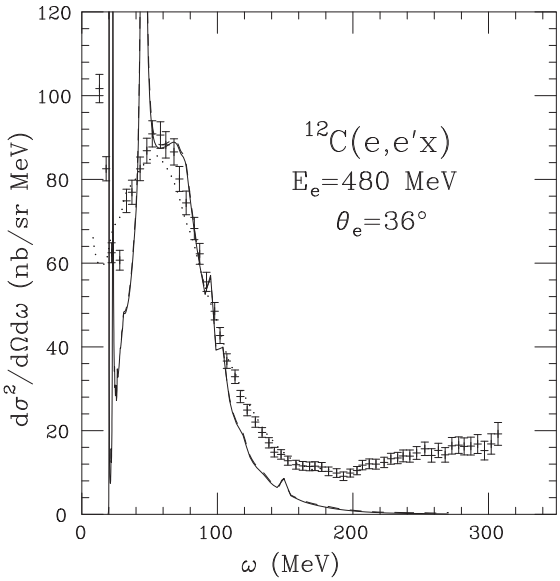

FIG. 8. Cross section for ^{12}C(e,$e'x$). The solid curve is from calculation with single-particle operators [Eqs. (10)–(12)]. The dashed curve includes meson exchange contribution. The dotted line results from using the 300 MeV/c responses in Fig. 9 that were extracted from data. Data are from Ref. [30].

states are removed from the basis. This is the high-energy octupole resonance. Its appearance at $106/A^{1/3}$ is consistent with the $110/A^{1/3}$ extracted from proton scattering on ^{40}Ca, ^{116}Sn, and ^{208}Pb [31]. It exhausts about one-half of the sum rule. Of course, an octuple resonance in ^{12}C would have a very large α-decay width, so such a narrow resonance would not show in the data. However, if its strength is spread over a width of 20 to 25 MeV, it would fill in what appears to be missing strength in this region. Such strength would be missing in any quasifree or optical model calculation of this process. It would be very beneficial to have $(\pi^+, \pi^{+\prime}p)/(\pi^-, \pi^{-\prime}p)$ data in this region. It was shown in Ref. [32] that this reaction can identify regions of giant resonances.

The transverse and longitudinal responses were extracted from the data in Ref. [30]. These are shown in Fig. 9 along with the calculations with single-particle operators shown as solid lines. The apparent weakness in the low-energy shoulder of the calculated transverse response at $q = 300$ MeV/c may not be real. In the analysis of the data, the energy resolution will mix the effect of the resonances and even bound states into neighboring energy regions, making the low-energy continuum response appear large. This result can be seen when the responses extracted from the data are entered into Eq. (5). The resulting cross section shown as a dotted line in Fig. 8 appears, and it does not track the apparent resonance at low energy.

In Fig. 10 is shown the data of Ref. [30] at $E_e = 680$ MeV and $\theta = 36^\circ$ compared to the calculated results both with (dashed line) and without MEC (solid line). This data set

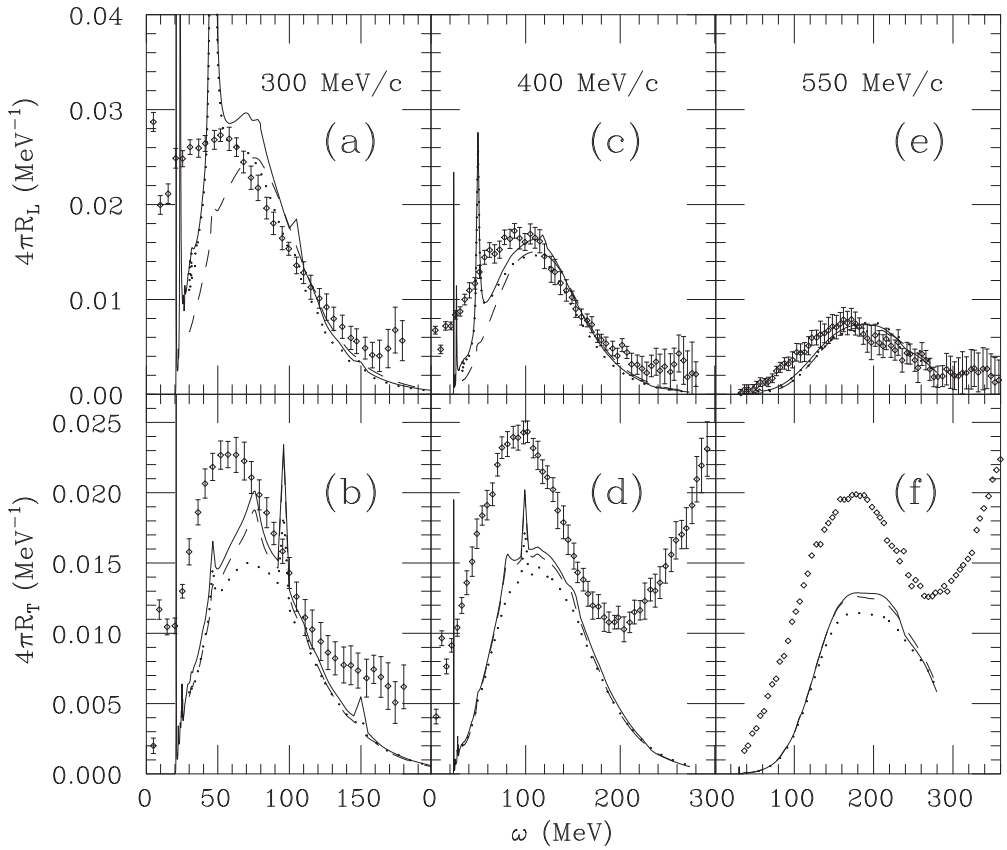

FIG. 9. Longitudinal and transverse responses extracted from the data of Ref. [30]. Solid lines are responses calculated with single-particle operators of Eqs. (10)–(12). Dashed lines omit contributions from coupled channels. Dotted lines omit contributions from 0s hole components.

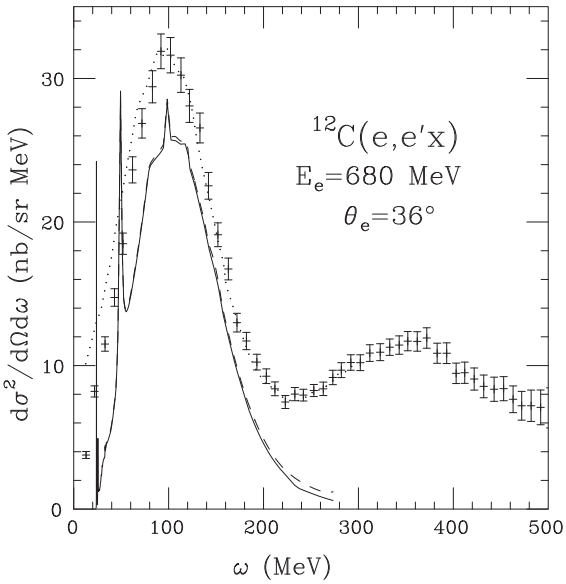

FIG. 10. Cross section for ^{12}C(e,$e'x$). The solid curve is from calculation with single-particle operators [Eqs. (10)–(12)]. The dashed curve includes meson exchange contribution. The dotted line results from using the 400 MeV/c responses in Fig. 9 that were extracted from data. Data are from Ref. [30].

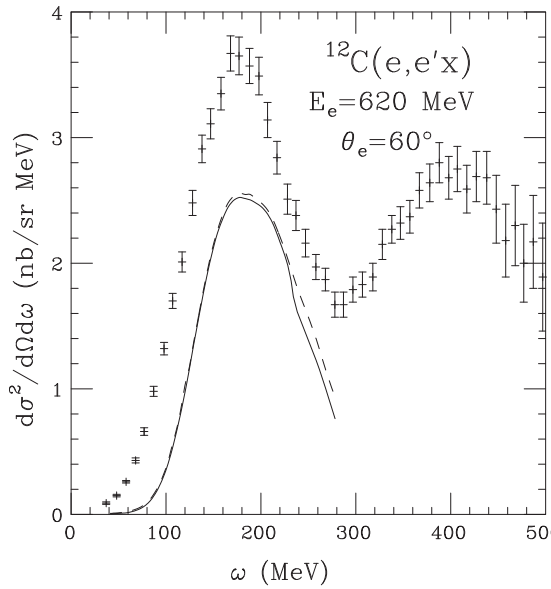

FIG. 11. Cross section for ^{12}C(e,$e'x$). The solid curve is from calculation with single-particle operators [Eqs. (10)–(12)]. The dashed curve includes meson exchange contribution. Data are from Ref. [30].

corresponds to an average q of ∼400 MeV/c. The position and width of the calculated quasielastic peak are in agreement with the data, but the peak cross section is now too small. The transverse-longitudinal response analysis shown in Fig. 9 indicates that the weakness is in the transverse response; however, the weakness at low energy may again be exaggerated because employing the responses from the data in Eq. (5) leads to a cross section that is too large at low energy, as shown by the dotted line in Fig. 10. The contribution of MEC, shown as the dashed line in Fig. 10, is too small to provide agreement with the data. A small contribution of the MEC was also found in Ref. [21]. This is in contrast to ^{4}He, where MEC in the RCCSM gives agreement with the data.

The cross section in Fig. 11 has a mean q of ∼550 Me/c, and here the data of Ref. [30] is poorly fit. The response function analysis for $q = 550$ MeV/c in Fig. 9 again points to the transverse response as being the main deficit. This effect, of the models that fit the transverse response at low q underpredicting the transverse response with increasing q, is the prevalent result. Also, the contribution of the resonances disappears at high momentum transfer, leaving the longitudinal response also too small in the low-energy region.

The contributions to the responses have been dissected in Fig. 9. The solid lines are the single-particle operator contributions. The dashed lines eliminate the contribution of channels that are not in the exit channel. This means that in Eq. (3) all c' contributions are set to zero unless $c = c'$. One can see that a large amount of the longitudinal response at $q = 300$ MeV/c is eliminated. This demonstrates a significant difficulty with optical model calculations of knockout reactions. In the optical model, elastic cross sections are fit by including absorption, which reduces the flux and, hence, the wave function in channel c. In the RCCSM elastic cross sections are fit by removing the flux in channel c by sending it to other channels. However, these channels contribute to the knockout process and are missing in optical model calculations. The contribution of the coupled channels diminishes with increasing q. Interestingly, the contribution of the high-energy quadruple resonance almost disappears without the coupled channels, showing that this resonance is, indeed, a collective excitation.

The dotted line in Fig. 9 results from eliminating the contribution of the 0s hole state component of the wave function. (They are still in the Hamiltonian; their amplitudes are just set to zero in the wave function.) They contribute over the range of q and have more effect than the MEC shown as dashed lines in Fig. 12.

Also included in Fig. 12 as dotted lines are the transverse responses calculated with only p-shell states included in the $A = 11$ basis. This allows one to address the effect of including higher $\hbar\omega$ states in ^{12}C. In Ref. [33] a marked improvement in the transverse response for the $2^+(4.44)$ was obtained by including a $0\hbar\omega$ plus $1\hbar\omega$ basis. The deficiency of the $0\hbar\omega$ space is demonstrated in Fig. 13, where the dashed line is the result with the Cohen and Kurath (8-16) interaction [8] as employed in Ref. [33]. Neither the nucleon form factor or center-of-mass correction is applied to this calculation. Shown as a dotted line is the equivalent calculation with the interaction in this present work. This demonstrates considerable dependence on the interaction. However, the peak of the response remains shifted to high q as compared to the data of Refs. [34] and [35]. The reason for this shift is that no contribution to the convection current can come from a pure p-shell calculation. Only the magnetization current contributes. Higher $\hbar\omega$ excitations are required to produce a convection current contribution, and, as observed in Ref. [33],

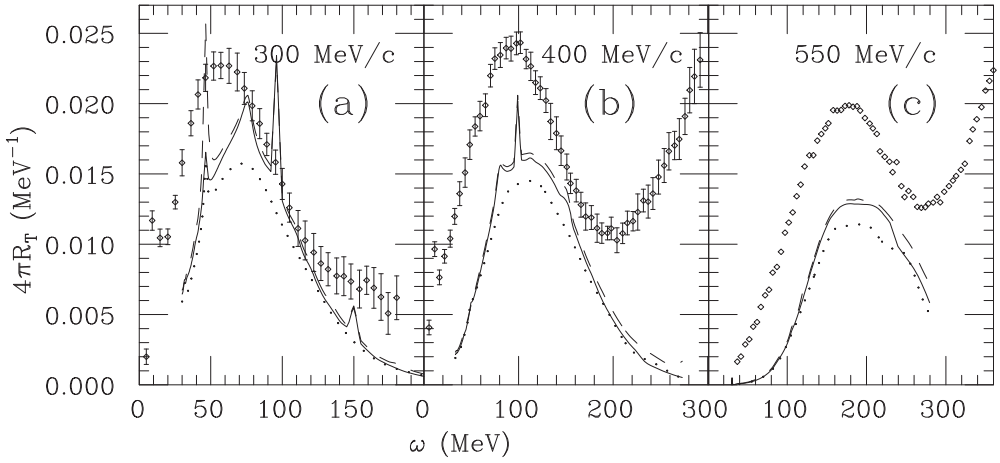

FIG. 12. The transverse responses extracted from the data of Ref. [30]. Solid lines are responses calculated with single-particle operators of Eqs. (10)–(12). Dashed lines include MECs. Dotted curves result from eliminating $1\hbar\omega$ states from the core states.

inclusion of the $1\ \hbar\omega$ space increased the strength and shifted the peak in better agreement with the data. However, the transverse response was still a factor of 2.5 too low. The addition of the $1\hbar\omega$ space was not sufficient to account for the complexity of this low-lying collective state.

The solid line in Fig. 13 is the result of the basis employed in this present work. The basis includes selected many-$\hbar\omega$ excitations from the $0s$ and $0p$ shells owing to working in the center-of-mass coordinate. The results are, however, very similar to those of Ref. [33], in that the peak has shifted, but the full strength has not been obtained. Therefore, the higher $\hbar\omega$ states improve the transverse response for this bound state, but it is not clear that improvement would be found for knockout reactions, because this process seems very different. Knockout at high energy and momentum transfer is primarily a single-nucleon process, whereas electroexcitation of bound states can involve collective motion. Indeed, if one compares the dotted lines in Fig. 9, where the $0s$-hole states were included in the $A = 11$ basis but their contribution set to zero, with the dotted line in Fig 12, where they were eliminated from the basis entirely, one sees only small differences. The primary effect of including the higher $\hbar\omega$ excitations in the basis is to allow $0s$-shell knockout, i.e., providing additional nucleons to hit, and this is not sufficient to account for the measured transverse response at high momentum transfer. A possible explanation for the remaining discrepancy follows.

VI. THE RECOIL TERMS

The above calculations follow the general trend of previous calculations in that the calculated transverse response at the higher momentum transfer is smaller than that extracted from data. This section presents a possible source of the deficit. This problem does not occur in ^{4}He where RCCSM calculations agree well with nearly all electron data [25]. Having the problem occur in the heavier ^{12}C system would lead one to guess that this is a medium modification effect. However, some crucial recoil terms are included in the ^{4}He calculation that are missing in the ^{12}C calculation and missing from other calculations in the literature. The effect of omitting these terms in ^{4}He is similar to the effect seen above in ^{12}C; i.e., the calculated transverse response is more suppressed as the momentum transfer increases. The recoil terms are negligible at $q \sim 205$ MeV/c but increase the 180° cross section by a factor of 2.4 at $q \sim 380$ MeV/c.

To see where the recoil terms arise, one can look at how the matrix elements of the single-particle operators are calculated

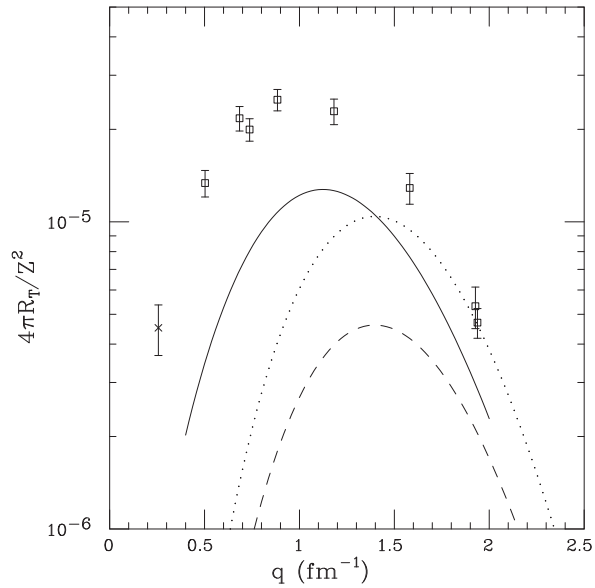

FIG. 13. Transverse reponse for ^{12}C(2^+), 4.44-MeV state. The dashed line is result for a p-shell calculation with Cohen and Kurath (8-16); the dotted line is result for p shell a calculation with the interaction in present work; the solid line is for full basis with the interaction in the present work. Open squares are data of Ref. [34]; the cross is a datum of Ref. [35].

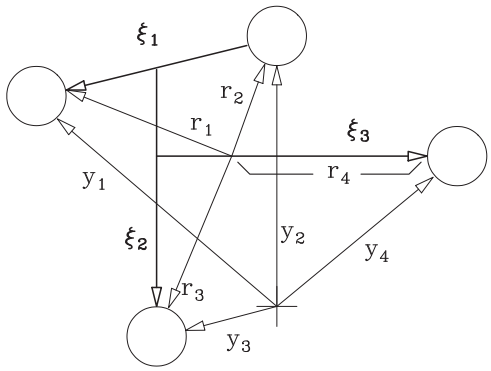

FIG. 14. The RCCSM coordinate system for ^{4}He.

for ^{12}C in this work. First, coefficients of fractional parentage of the ^{12}C p-shell states are employed so that all components of the initial- and final-state wave functions of Eq. (1) are written as a sum of oscillators coupled to core states:

$$\Psi_{J_B} = \sum_{J_A \alpha \bar{l} \bar{j} \bar{n}} g_{\bar{n}\bar{l}\bar{j} J_A \alpha J_B} [\varphi_{\bar{n}\bar{l}\bar{j}}(\xi) \otimes |\alpha J_A\rangle]^{J_B}. \quad (15)$$

The oscillators are a function of the coordinate connecting the center of mass of the core and the particle and have oscillator constant $\nu = \nu_0(A-1)/A$. Matrix elements of single-particle operators are taken to be diagonal in the core states and connect the particle states. This would be the same procedure used in optical model calculations. Next, it is instructive to look at the coordinate system for ^{4}He shown in Fig. 14. The RCCSM creates a particle in coordinate $\boldsymbol{\xi}_3$ as in Eqs. (1) and (15).

The single-particle operators in Eqs. (10)–(12) require coordinates $\mathbf{r}_1$, $\mathbf{r}_2$, $\mathbf{r}_3$, and $\mathbf{r}_4$, and $\mathbf{r}_1 = 3/4\boldsymbol{\xi}_3$. Hence, a first correction is to use $\mathbf{r}_1 = (A-1)/A\xi_3$ in these equations. This can make up to a 10% effect in ^{12}C for the reactions considered here. However, the single-particle operator sums all particles, and coordinates $\mathbf{r}_1$, $\mathbf{r}_2$, and $\mathbf{r}_3$ must also be included. These could be included exactly in the simple $0s^3$ model of ^{3}H and ^{3}He. Comparing of the results of Ref. [36] where the RCCSM wave functions were treated as particle-hole wave functions, and hence included only $\mathbf{r}_4$, with the results of Ref. [25], where all Jacobi coordinates were used, one sees that including the recoil terms causes the 180° cross sections (and hence the transverse response) to increase with increasing momentum transfer. The recoil terms were absolutely necessary for agreement with the data. One could argue that such a recoil effect would be small in the heavier ^{12}C system. However, ^{12}C has many more particles to contribute, so the situation is not clear.

VII. CONCLUSION

The RCCSM has been extended to include core states with $1\hbar\omega$ excitations. This extension allows one to include $0s$-shell knockout processes. The model was applied to the ^{11}B$(p,n)^{11}$C and ^{11}B$(p,p')^{11}$B reactions, and reasonable agreement with available data was obtained. Successful ^{11}B$(p,n)^{11}$C calculations provide confidence in the model's ability to predict cross sections to proton-rich systems. The calculated elastic proton scattering cross section at 30.3 MeV agrees well with the data; however, the calculation at 155 MeV gives the appearance that the target size is somewhat too small.

Calculations were performed for ^{12}C$(e,e'x)$ in the quasi-elastic region. The agreement with measured cross sections was good at low-momentum transfer. At high q, the calculated cross sections were smaller than the data, and dissection of the cross sections into longitudinal and transverse responses indicated that the weakness was in the transverse response. A possible explanation for this lack of strength is the neglect of recoil terms. Elimination of the contribution of coupled channels reduces the longitudinal response by 23% at $q = 300$ MeV/c, but only 2% at $q = 550$ MeV/c. Appearing at an energy of $106/A^{1/3}$ MeV is the high-energy octupole resonance. It contributes a significant amount of strength to the longitudinal response at $q = 300$ MeV/c. Such a contribution would be missing from optical model calculations.

The inclusion of $0s$ shell knockout is less significant, but its contribution persists throughout the range of momentum transfer. The contribution of MEC is smaller than those calculated for ^{4}He in Ref. [25] and are not sufficient to boost the calculated cross section in agreement with the data. The ability of RCCSM calculations to describe the ^{12}C$(e,e'x)$ reaction at and below 300 MeV/c indicates that they should provide useful predictions for other knockout reactions in this momentum-transfer region.

ACKNOWLEDGMENT

This work was supported by the National Science Foundation under Grant No. PHY-0855339.

APPENDIX

The effective interaction employs the same form and ranges as in Ref. [37]. The central components are given by $V = \sum_{i=1}^{3} V_i Y(r/R_i)$, the spin-orbit components by $V = \sum_{i=1}^{2} V_i Y(r/R_i)\ \boldsymbol{L}\cdot\boldsymbol{S}$, and the tensor components by $V = \sum_{i=1}^{2} V_i r^2 Y(r/R_i)\ \mathrm{S}_{12}$, with $Y(x) = e^{-x}/x$. The coefficients, V_i, are given in Table II.

TABLE II. Effective interactions strengths, V_i.

Force	Range (fm)	Triplet even (MeV)	Triplet odd (MeV)	Singlet even (MeV)	Singlet odd (MeV)
Central	0.25	21 599.80	−1000.00	4954.80	1254.50
	0.40	−6342.00	1217.60	−1862.20	452.5
	1.414	−10.46	0	−10.463	0
Spin-orbit	0.25	−1000.00	9999.80		
	0.40	−2998.60	−2592.10		
Tensor	0.40	−1869.20	483.00		
	0.70	59.59	13.62		

[1] R. J. Philpott, Nucl. Phys. A **289**, 109 (1977).
[2] D. Halderson, Int. J. Mod. Phys. E **14**, 171 (2005).
[3] R. J. Philpott, Nucl. Phys. A **243**, 260 (1975) and references therein.
[4] P. Descouvemont, Rep. Prog. Phys. **73**, 036301 (2010).
[5] D. Halderson, Phys. Rev. C **73**, 024612 (2006).
[6] J. Grineviciute and D. Halderson, J. Phys. G **35**, 055201 (2008).
[7] D. Halderson, Nucl. Phys. A **707**, 65 (2002).
[8] D. Halderson, R. J. Philpott, J. A. Carr, and F. Petrovich, Phys. Rev. C **24**, 1095 (1981).
[9] Nushell@MSU, B. A. Brown, and W. D. M. Rae, MSU-NSCL Report, 2007.
[10] S. Cohen and D. Kurath, Nucl. Phys. A **73**, 1 (1965).
[11] R. V. Reid, Jr., Ann. Phys. (NY) **50**, 411 (1968).
[12] A. S. Clough, C. J. Batty, B. E. Bonner, and L. E. Williams, Nucl. Phys. A **143**, 385 (1970).
[13] J. F. Cavaignac, S. Jang, and D. H. Worledge, Nucl. Phys. A **243**, 349 (1975).
[14] J. Lowe, Nucl. Phys. A **162**, 438 (1971).
[15] B. Gepffrion, N. Marty, B. Tatischeff, and A. Willis, Nucl. Phys. A **116**, 209 (1968).
[16] O. Benhar, D. Day, and I. Sick, Rev. Mod. Phys. **80**, 189 (2008).
[17] J. W. Van Orden and T. W. Donnelly, Ann. Phys. **131**, 4 (1981).
[18] G. Co, K. F. Quader, R. D. Smith, and J. Wambach, Nucl. Phys. A **485**, 61 (1988).
[19] J. Jaenicke, P. Schuck, and R. W. Hasse, Phys. Lett. B **214**, 1 (1988).
[20] M. Cavinato, D. Drechsel, E. Fein, M. Marangoni, and A. M. Sarius, Nucl. Phys. A **423**, 376 (1984).
[21] J. C. Caillon and J. Labarsouque, Nucl. Phys. A **595**, 189 (1995).
[22] C. J. Horowitz and J. Piekarewicz, Nucl. Phys. A **511**, 461 (1990).
[23] J. E. Amaro, G. Co', and A. M. Lallena, Ann. Phys. **221**, 306 (1993).
[24] V. De Donno, M. Anguiano, G. Co', and A. M. Lallena, Phys. Rev. C **84**, 037306 (2011).
[25] D. Halderson, Phys. Rev. C **53**, 2978 (1996).
[26] T. de Forest, Jr. and J. D. Walecka, Adv. Phys. **15**, 1 (1965).
[27] T. Janssens, R. Hofstadter, E. B. Hughes, and M. R. Yearian, Phys. Rev. **142**, 922 (1966).
[28] D. J. Dubach, J. H. Koch, and T. W. Donnelly, Nucl. Phys. A **279**, 279 (1974).
[29] D. T. Baran, Ph.D. thesis, Northwestern University, 1989.
[30] P. Barreau *et al*., Nucl. Phys. A **402**, 515 (1983).
[31] T. A. Carey, W. D. Cornelius, N. J. DiGiacomo, J. M. Moss, G. S. Adams, J. B. McClelland, G. Pauletta, C. Whitten, M. Gazzaly, N. Hintz, and C. Glashausser, Phys. Rev. Lett. **45**, 239 (1980).
[32] D. Halderson and V. A. Sadovnikova, Phys. Rev. C **56**, 2688 (1997).
[33] S. Karataglidis, P. Halse, and K. Amos, Phys. Rev. C **51**, 2494 (1995).
[34] J. B. Flanz, R. S. Hicks, R. A. Lindgren, G. A. Peterson, A. Hotta, B. Parker, and R. C. York, Phys. Rev. Lett. **41**, 1642 (1978).
[35] P. Strehl, Z. Phys. **234**, 416 (1970).
[36] A. Hotta, J. Dubach, R. S. Hicks, R. L. Huffman, B. Parker, G. A. Peterson, P. J. Ryan, R. P. Singhal, and D. Halderson, Phys. Rev. C **38**, 1547 (1988).
[37] D. Halderson, J. Phys. G **20**, 1461 (1994).